Modeling Free-Stream Turbulence based on Wind Tunnel and Flight Data for Instability Studies

T.K. Sengupta*, D. Das, P. Mohanamuraly, V.K. Suman and A. Biswas
Department of Aerospace Engineering, Indian Institute of Technology, Kanpur, India
*tksen@iitk.ac.in, Phone: 91-512-2597945, FAX: 91-512-2597561

Abstract

Present research was initiated to study the effects of free stream turbulence (FST) on flow instability and transition. In the past, instabilities of several flows were investigated experimentally with respect to FST. Theoretical model for FST is developed here that matches higher order statistics of data obtained from wind tunnel and flight test experiments. The developed model is applied for studying numerically, the effect of FST on onset of Karman vortex shedding for flow past a circular cylinder that match well with available experimental data.

1. INTRODUCTION

Understanding the roles of FST on onset of instabilities for streamlined bodies and on separation-initiation for bluff body flows are fundamentally and practically important. One such phenomenon is the stall noted in the flow over aircraft wing in clear air due to small scale atmospheric turbulence [1]. Mild to moderate stall, due to atmospheric turbulence (of larger length and time scales) and clear air turbulence (of space and time scales those are relatively smaller), are experienced by almost all aircrafts. However, detailed in-flight experimental data are not available correlating stall with FST. An appropriate mathematical model of atmospheric FST is necessary to investigate these effects computationally on the flow field over an aircraft wing. Several studies on FST of wind tunnels exist with a view to design tunnels [2-8]. Similarly, studies also exist pertaining to the role of FST on unsteady separated flow over turbo-machine blades (see [9] for further references). Usually FST levels of flows in turbo-machineries are significantly larger than FST levels noted in wind tunnels and in free-flight over aircrafts.

Meuller et al. [10] have studied the effects of FST on lift and drag of low Reynolds number flow (in the range of 10^5 to 10^6) over an airfoil. They reported that for Reynolds number below 2×10^5, the boundary layer is extremely sensitive to the amplitude and the frequency content of FST. To understand this phenomenon in a quantitative manner via theoretical and computational approaches, it is necessary to correlate the background disturbance with the response of the flow. Both wind tunnel and free flight turbulence can be characterized by the probability distribution functions (PDF) of the velocity time series that can be used to obtain turbulence intensity and other higher order statistics [11]. In addition, structural vibrations present in the model and the prototype, in wind tunnel [10] and in flight, respectively can also display features similar to those due to FST.

Kwok [12] experimentally studied the effects of FST, particularly the small-scale turbulence on flow past a smooth cylinder, in the Reynolds number range of 8.3×10^4 to 5.5×10^5. Wind tunnel tests, under smooth and rod-generated turbulent flows, show [12] that increase in FST promotes early transition and a delay in flow separation, resulting in modification of the mean pressure distribution and reduction in drag. The author suggested that only the small-scale turbulence near the stagnation line of the cylinder is primarily responsible in producing these effects.

Pal & Raj [13] studied the behavior of the wake of a thin and smooth flat plate in the presence of FST for Reynolds number ranging between 2.07×10^5 and 2.56×10^5 and for the specific FST intensity (as defined in equation (3)) of 0.4 %, 5.0 % and 7.23 %. Based on similarity hypothesis, they obtained two parameters of FST, in self-similar wakes, and showed from their experiments that these parameters are dominant in the near-wake region only.

Since FST strongly influences results in many studies, endeavours have been taken to create a smoother and more uniform flow in wind tunnels. Taylor & Batchelor [2] have shown that increase in

the number of screens decrease the turbulence levels. Baines and Peterson [3] have investigated the role of the screens and the perforated plates on free stream flow and turbulence modification in a wind tunnel. Lumley & Mc Mohan [4] have demonstrated the substantial reduction in turbulence levels in a water tunnel by the use of honeycombs. Suppression and generation of FST with the help of honeycombs is studied also by Loehrke & Nagib [5]. Mikhailova et al. [6] have studied the effects of the location and the geometry of honeycombs in fixing FST of a wind tunnel. Derbunovich et al. [7] investigated the optimal shapes and sizes of the screens and their location to minimize FST in a wind tunnel test section. Schmid et al. [8] obtained low FST levels (< 1%) in a wind tunnel by using fibrous mats and a packed bed of different porosity, upstream of the contraction.

In real flows, omnipresent FST with low amplitude of excitation can trigger transition to turbulence via the creation of deterministic waves. However, FST in general, appears as a random non-deterministic event that can only be modeled stochastically, at present. As noted here with respect to flow instability past a circular cylinder, the description of FST and specifically the amplitude of it, near the Strouhal frequency, are necessary. In a computational framework, a combination of deterministic and stochastic approaches is required to understand the effects of FST. Here, an attempt has been made to model FST using the higher order statistics of the disturbance-field. In a statistical description of turbulence, variance or the second order statistics represents the magnitude of turbulent fluctuations; skewness or the third order statistics represents deviations from symmetric distribution; kurtosis or the fourth order statistics describes the flatness of the tail of the distribution. It is easy to extract the statistics of turbulence experimentally; however, a realistic reconstruction of FST that can be used in a mathematical model requires additional information on lower frequency contents of the velocity signal. In this study, a mathematical model of FST is presented by incorporating these statistical quantities and the frequency contents of FST data calculated from wind tunnel and flight experiments. The role of FST on the onset of instability for flow past circular cylinder is demonstrated through experiments and verified with the numerical calculation of the Navier-Stokes equations by using the proposed FST model.

In an alternate approach, Lucor & Karniadakis [14] simulated the effects of time-dependent inflow as a stochastic laminar flow created by a uniform flow along with uniformly distributed random disturbances. In Sengupta et al. [15], a model of FST was developed, on the basis of published wind-tunnel data (Frisch [16]) for studying chaotic-dynamics and intermittency of flow past an aerofoil at high angles of attack for moderate Reynolds numbers. The FST model was developed using the second and the fourth moments of experimental data [16], to capture the essential dynamics involving flow instabilities and stochastic forcing.

Spark & Dutton [17] demonstrated a possible way of simulating turbulence using phase angles associated with the Fourier transform of a random time series. They considered an arbitrary random disturbance of Gaussian distribution and obtained the Fourier transform of the synthetic time series. Finally, they replaced the original energy spectrum with a -5/3 spectrum in the inertial range. To further include the phase information they assumed that the intermittent behaviour of FST is given by delta functions at discrete times that help in providing the correct phase information of oncoming turbulence. Similar models with uniformly distributed phase angles were also used by Edwards [18] and Syono & Tanaka [19] who did not include the -5/3 spectrum information.

Experimentally obtained critical Reynolds number (Re_{cr}) for the onset of Karman vortex shedding (KVS) in flow past a cylinder is facility dependent data – as reported by different authors. Batchelor [20] conjectured this value to be between 30 and 40. Landau & Lifschitz [21], very specifically noted: "*The critical Reynolds number is not, of course, a universal constant, but takes a different value for each type of flow. …. For example, in flow across a cylinder undamped non-steady flow has been observed for R = ud/n = 34, d being the diameter of the cylinder*". Other experimental records also show large scatter with Re_{cr} varying between 40 [22] and 65.2 [23]. It is noted that in Homann's [22] experiments, the flow was created in a highly viscous oil as the working fluid and that reported the highest Re_{cr} value. No shedding of vortices below Re = 65.2 was observed in this study. Highly viscous oil causes higher dissipation of background disturbances, lack of which does not lead to shedding. Otherwise, from different experiments performed with different facilities, one notes critical Reynolds numbers varying from 40 to 53 [22, 24-25]. These experimental values significantly differ from those reported in Hopf-bifurcation studies [26-27] that identify a Re between 45 and 46 as the critical Reynolds number. This is indicated by the global temporal linear instability of a steady flow around the circular cylinder, linking bifurcation with linear instability. The experimental values of Re_{cr} are related to the receptivity of the actual flow with respect to the prevalent background disturbances in the facility,

thereby accounting for the large scatter. Very little attention has been paid to this aspect of the flow in theoretical studies- mostly due to the absence of a realistic model for background disturbances. This is the primary motivation behind the present study.

2. CHARACTERIZATION OF WIND TUNNEL FST

The importance of FST is noted from the experimental results shown in Figure 1a, where two flows have been compared for the flow past a circular cylinder at the same Reynolds number Re = 53, obtained by taking two cylinders of diameters 5mm and 1.8mm placed in different uniform flows- at speeds indicated in the figure. This result establishes that experiments performed in the same tunnel, at varying freestream velocity, while keeping the Reynolds number same, give rise to different shedding patterns (as shown in the top frames in Figure 1a), highlighting the role of FST on shedding. It is noted that empty tunnel FST levels are strong functions of flow speed- as shown in the FFT of empty tunnel velocity time series in the bottom frames of Figure 1a. Empty tunnel FST has been measured in all the cases at the location of the tested model. Different shedding patterns can be explained by noting that the applied background disturbances at the same Reynolds number and the same Strouhal number are different for different free stream speed- as shown in the bottom frames of Figure 1a, by the spectra of the empty tunnel noise data. The shedding pattern for the flow past cylinder is characterized by its non-dimensional frequency or the Strouhal number (St) and for Re = 53, it is given by $St \approx 0.124$ [28] (Schlichting 1979). The physical frequency at the Strouhal number (f_{st}) for the cases of Figure 1a work out as $f_{st} \approx 4$Hz for U = 17cm/s and $f_{st} \approx 31$Hz for U = 46.9cm/s. From the detailed spectra at very low frequencies shown in

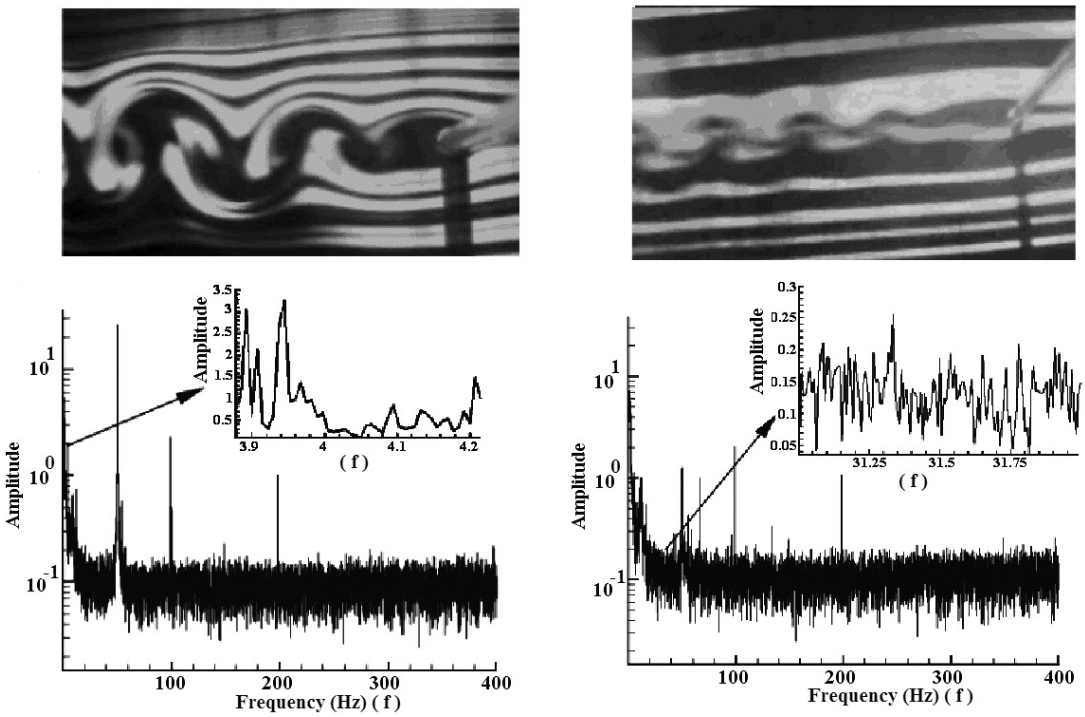

Figure 1a. Experimentally observed flow past a cylinder for Re = 53 with (i) U = 17 cm/s, D = 5mm, f_{st} = 4Hz and (ii) U = 46.9 cm/s, D = 1.8mm, f_{st} = 31Hz. FFT of empty-tunnel disturbance field shown below the visualization pictures at the same speed with the inserts showing amplitude near the Strouhal frequency.

Figure 1a, one observes that the amplitude of FST for U =17cm/s near the Strouhal frequency is 3.3, that is more than ten-times the amplitude of FST for U = 46.9cm/s- for which the corresponding amplitude is only 0.27. Hence, U = 17cm/s case showed stronger receptivity, leading to well defined vortex shedding pattern. In comparison, for the higher speed the excitation being weaker, the

corresponding shedding pattern is also weak. This establishes the relevance of background disturbance upon flow instability and vortex shedding at the natural frequency (f_{st}). Thus, the flow receptivity depends upon Re and *Tu* (at f_{st}) – where *Tu* is defined as in Equation (3); Re determines the transfer function of the fluid dynamical system and *Tu* at f_{st} is the corresponding input to the dynamical system at its natural frequency.

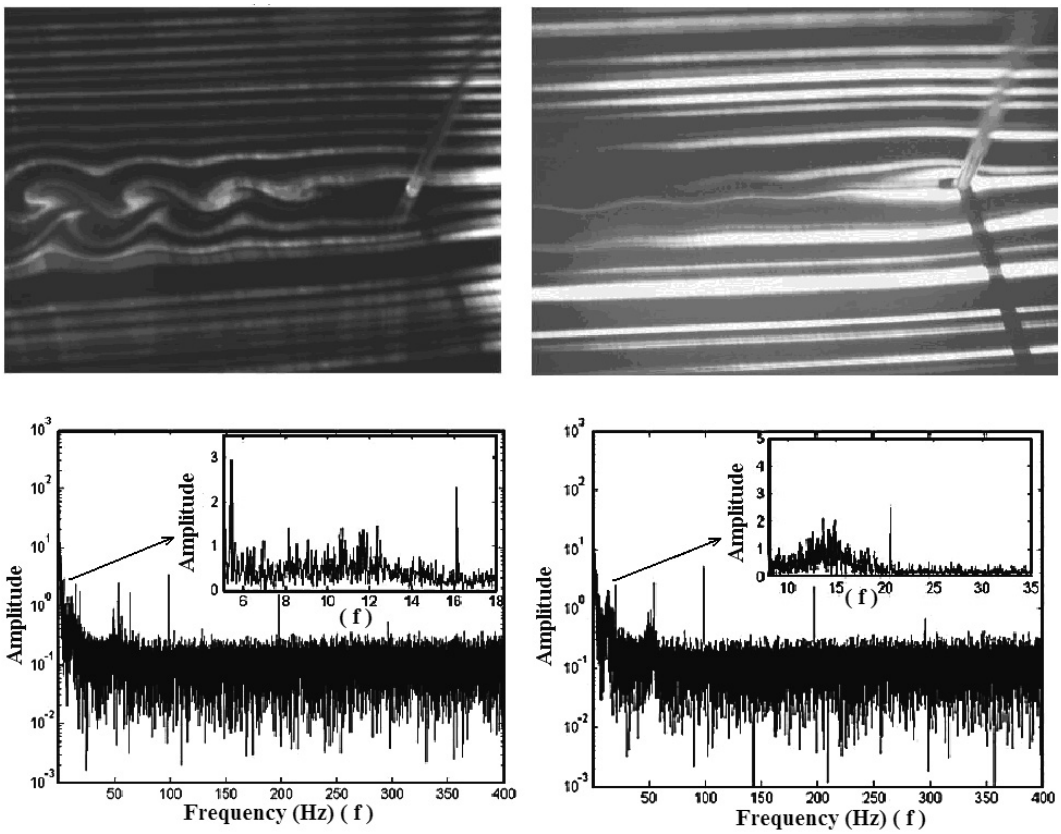

Figure 1b. Experimentally observed flow past a cylinder for Re = 45 with (i) U = 26.1 cm/s, D = 2.6mm, f_{st} = 11.8Hz and (ii) U = 37.8 cm/s, D = 1.8mm, f_{st} = 24.8Hz. FFT of empty-tunnel disturbance field are shown below the visualization pictures at the same speed with the inserts showing amplitude near the Strouhal frequency.

Similar conclusions can also be reached from the comparison of cases shown in Figure 1b for Re = 45. In these cases, flow speeds are not too different and the disturbance velocity amplitudes are also similar with some fine distinctions only at lower frequencies. For one of the cases shown in Figure 1b (i): with U =26.1cm/s and Strouhal number *St* = 0.11, the corresponding physical frequency is $f_{st} \approx$ 11.8Hz, at which the FST amplitude is more than 1. For the other case shown in Figure 1b (ii): with U =37.8cm/s and the same Strouhal number, the corresponding physical frequency is 24.8 Hz, at which the FST amplitude is less than 0.25. The difference in amplitudes of input disturbances at f_{st} explains once again the higher receptivity of the flow at the lower speed.

To characterize wind tunnel FST, freestream velocity is measured in a low speed wind tunnel without any model- shown as the empty-tunnel records in Figures 1a and 1b. The wind tunnel used for the present work is shown in Figure 2- an open-circuit tunnel with test-section measuring 30cm X 40cm and with a contraction ratio of 9:1. It has six screens and a honeycomb upstream of the test section.

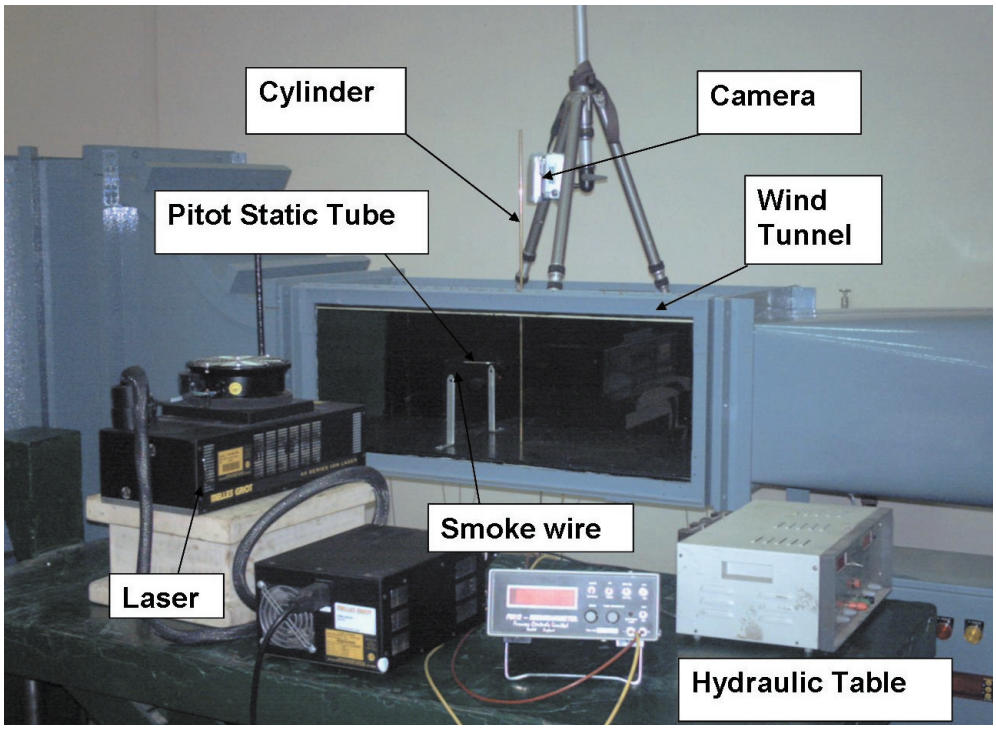

Figure 2. Photograph of the test section of the wind tunnel along with flow visualization arrangements.

The model is placed at the center of the test section with respect to the horizontal and the spanwise direction. The smoke wire arrangement is supported by two struts of symmetric airfoil sections with a distance of 24cm between them. Also the smoke wire arrangement is placed 15cm upstream of the circular cylinder model, ensuring that there are no influences of these system with the vortex shedding by circular cylinder. In the same way the Pitot tube is above the smoke wire level which does not affect the vortex shedding. The straight smoke-lines in Figure1b clearly reveal the absence of such interferences.

A hotwire system of Dantec Dynamics is used to measure the streamwise velocity, with 60% overheat ratio. Emphasis is given upon the velocity range of 0.17m/s to 2m/s. To minimize the calibration error, three sets of calibration are carried out in the range of 0.17m/s to 0.5m/s; 0.5m/s to 1.0m/s and 1.0m/s to 2m/s. The calibration of the hotwire is carried out with reference to a Pitot tube connected with a micro-manometer with a dynamic range of 20Pa that is also used to measure the tunnel mean speed.

In Figure 3a, the measured empty-tunnel time series is shown for the wind-tunnel velocity of 17cm/s. Data have been sampled at 10kHz over a period of 40sec. Lower frequency components of the data in Figure 3a(i) have been filtered out and the high frequency fluctuations of the same have been shown in Figure 3a(ii). The long tail of the Fourier transform (not shown) of the data in Figure 3a(i), has contributions at higher frequencies that is due to electronic noise- as evident from the FFT of no-flow data presented in Figure 3b. Here, the time series is represented by its PDF, for the deviation from the mean. The PDF has been used to calculate up to the fourth order statistics.

Figure 4a shows the variation of wind tunnel velocity for the mean speed of 40.5cm/s, along with the PDF of the disturbance velocity and its FFT. The PDFs are plotted using Freedman-Diaconis rule [29] (Freedman & Diaconis 1981). This rule optimally chooses the bin-width based on the sample size and the spread of the data. It is evident that the PDF deviates significantly from a pure Gaussian distribution. Skewness (Sk) and Kurtosis (Ku) (third and fourth order statistics) are also calculated from the PDF using the following formulae,

$$Skewness(Sk) = \frac{E\left(u(t) - \bar{u}\right)^3}{\sigma^3} \tag{1}$$

$$\textit{Kurtosis}(Ku) = \frac{E\left(u(t) - \bar{u}\right)^4}{\sigma^4} \tag{2}$$

where, $\bar{u} = \frac{1}{T}\int_{t}^{t+T} u(t)dt$, is the mean of $u(t)$; σ is the standard deviation of $u(t)$; $E(\ .\ )$ represents the expected value of the corresponding argument. Turbulence intensity is calculated from the formula

$$\text{Tu} = \sqrt{\overline{u'^2}}/U_\infty \tag{3}$$

At a certain distance from the screens (along the centre of the tunnel test section) the turbulence is isotropic in nature and the r.m.s. fluctuations in the three directions are nearly equal (Schlichting [28], pp-470) i.e., $\overline{u'^2} = \overline{v'^2} = \overline{w'^2}$, where, $u'(t) = u(t) - \bar{u}$ It is for this reason, the empty-tunnel noise is characterized by measuring only the Streamwise component of the velocity.

The values of the various moments for the particular case of Figure 4(a) are Tu = 0.88%, Sk = 0.1238, and Ku = 2.9871. Thus, the skewness despite being small is non-negligible, and kurtosis differs slightly from the Gaussian distribution (3.0). The background disturbance data show that there are significant lower frequency contents, indicating presence of large scale, slowly varying, vortical structures that is known to destabilize flows. To find the statistical spread of different moments and the random nature of fluctuations, another set of data is presented in Figure 4b for the mean velocity 42cm/sec. The chosen velocity is very close to the previous case (as the error in the measurement of mean velocity is within 2%). There is rather small variations in Tu, as well as in Ku- but the skewness values are significantly different. Looking at the frequency contents in Figure 4a (iii) and 4b (iii), this difference can be attributed to differences at lower frequencies in the spectrum. Differences in the FFT plots are observed in the frequency-band of 2 to 6 Hz. It indicates that an appropriate representation of FST cannot be obtained through the description of the smallest scales alone. The accurate determination of all scales is indispensable for instability studies, because the large scale disturbances are mainly responsible in triggering instabilities. Similar low frequency contents in velocity signals have also been recorded in Frisch (Fig, - 3.1 Frisch [16]).

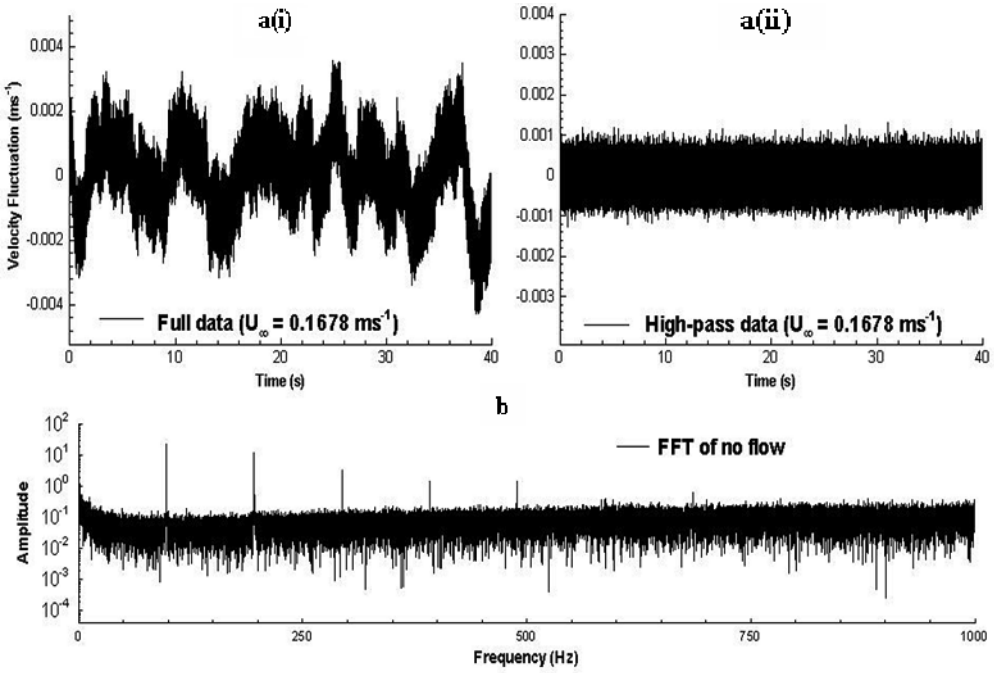

Figure 3. (a) Time series of empty-tunnel disturbance velocity (i) for full and (ii) high-pass data. (b) FFT of no-flow data (indicating electronic noise).

Figure 5a, b and c show results for the freestream velocities 50cm/s, 70cm/s and 99cm/s, respectively. Figures in each column show the velocity signal, corresponding PDF and FFT of disturbance velocity. Resembling features of PDFs are observed in Figure 4 indicating that the characteristics of the tunnel are similar in the velocity range 20cm/s to 1m/s. The nature of PDFs is not pure Gaussian, and turbulence intensities are of the order 1%. The skewness in PDFs is due to slowly varying large scale vortical structures. The peak in PDF is shifted from the centre indicating different values of skewness, a characteristic feature of the tunnel. Variations in PDFs can again be traced to differences at lower frequencies of the signal seen in FFT plots for all the cases. In FFT plots, a hump with maxima around 17Hz in Figures 4(a) (iii) and (b) (iii) denote a specific characteristic of this tunnel and it moves to higher values as the tunnel velocity increases. These maxima are seen to occur at 19Hz, 23Hz and 27Hz for the tunnel speed of 50cm/s, 70cm/s and 99cm/s, respectively. This occurrence of the maximum corresponds to fluctuations due to vortical flow created by the fan-blades, those are located downstream of the test section. The rotational speed of the 6-bladed fan is measured using a non-contact type optical tachometer and the blade frequency associated with the fan rotation is the blade passage frequency [10] in Figure 6. These frequencies correspond exactly to the humps in the FFT. The disturbance pressure waves created by the rotating fan-blades move upstream and contribute to the noise in the tunnel. Other lower frequency signature in disturbance velocity signal is seen within 70Hz in all the cases and can be attributed to tunnel inlet conditions, tunnel construction and flow control. Six screens of gradually decreasing sizes follow a flow straightener in this tunnel. The six-bladed fan is driven by a frequency controlled AC motor of 1.5kW and most of the low frequency characters of FST can be attributed to these components of the tunnel, though it is difficult to measure and characterize each of these components separately.

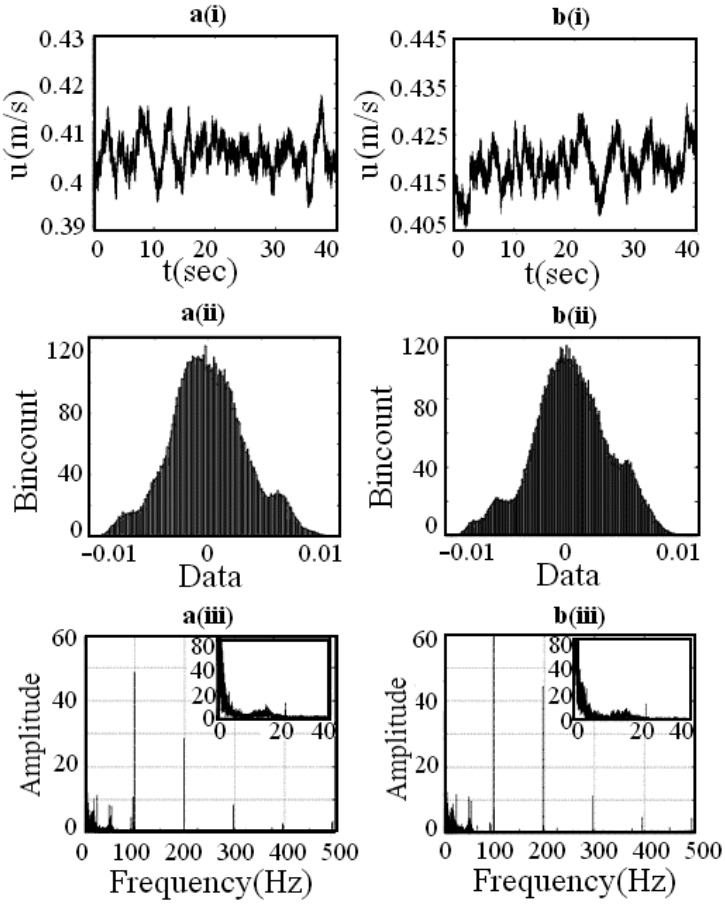

Figure 4. Characteristics of the wind tunnel at different freestream velocities: (i) Full velocity signal, (ii) PDF of disturbance velocity and (iii) FFT of (ii) for (a) U_∞ = 40.5 cm/sec, corresponding *Sk* = 0.1238, *Ku* = 2.9871, *Tu* = 0.88% and (b) U_∞ = 42 cm/sec and corresponding *Sk* = - 0.0859, *Ku* =2.867, *Tu* = 0.98%

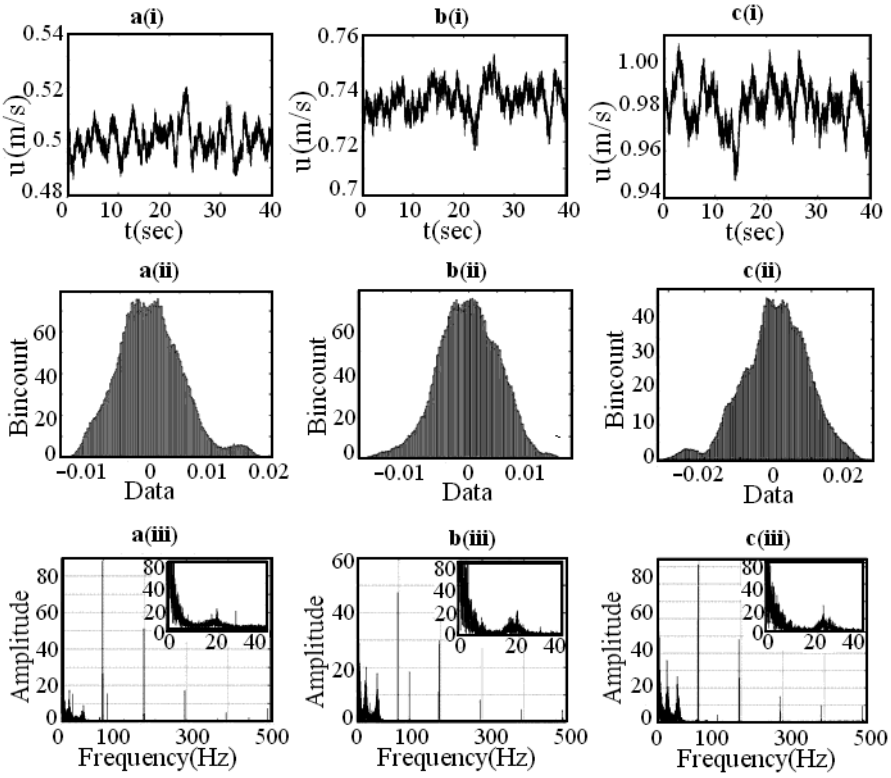

Figure 5. Characteristics of the wind tunnel for different freestream speeds: (i) Full velocity signal, (ii) PDF of disturbance velocity and (iii) FFT of (ii) for (a) U_∞ = 50 cm/sec, corresponding *Sk* = 0.3969, *Ku* = 3.268, *Tu* = 1.08% and (b) U_∞ = 70 cm/sec and corresponding *Sk* = -0.121, *Ku* = 2.962, *Tu* = 0.714% and (c) U_∞ = 99 cm/sec and corresponding *Sk* = -0.282, *Ku* = 3.156, *Tu* = 0.92%.

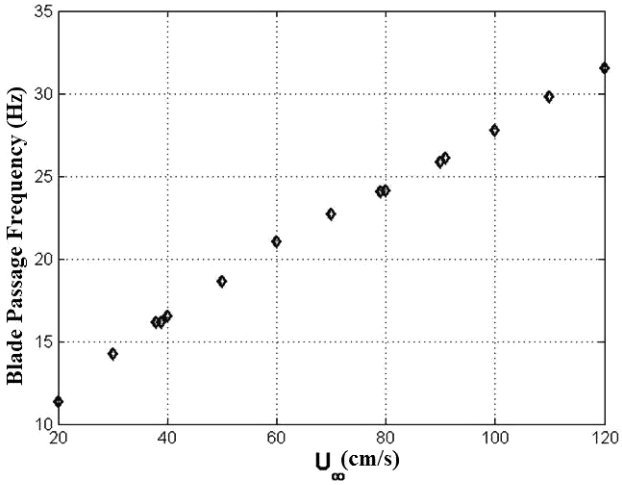

Figure 6. Variation of blade passage frequency with mean tunnel velocity.

3. CHARACTERIZATION OF FLIGHT DATA

Figure 7 shows the aircraft and the instruments used for the flight data recording of the equivalent oncoming flow speed. The aircraft used is the HANSA-3 aircraft of the Flight Laboratory, Aerospace Engineering Department, IIT Kanpur. Data is recorded with a mini air data boom (shown in Figure 7b) of SpaceAge Control Inc. (model 100400), made of aluminum body with a stainless steel nose of

6.35mm diameter and 196.85mm length. The boom measures static and total pressures, and the direction of the boom axis with respect to flow direction is measured with two tilt sensors. Two separate sets of data have been obtained in two different days at the same altitudes.

In Figures 8 and 9, the time series and its PDF, respectively are shown for the data collected from flight tests on April 4th 2007. Displayed time-series data of Figure 8 are obtained for the mean wind speed 36m/sec, 41.2m/s and 46m/s at the three altitudes of 2743.2m (9000ft), 1828.8m (6000ft) and 914.4m (3000ft), respectively. Data is sampled at 1 kHz for 8 to 25s depending on the duration of constant cruise speed at that particular altitude during a test flight. Corresponding PDFs are shown in Figure 9. It is noted that the PDFs of flight test data are also not symmetric, having significant number of events in the tail – implying the central role of higher order statistics of the associated FST measured by the time series. Similar nature of FST is observed in the measured data of Sept 9th 2007, shown in Figures 10 and 11. Data have been acquired at same altitudes and at similar mean speeds. It is noted that the data measured in the month of April (a completely dry season before the monsoon), has different statistics from the September-data that is affected by monsoon.

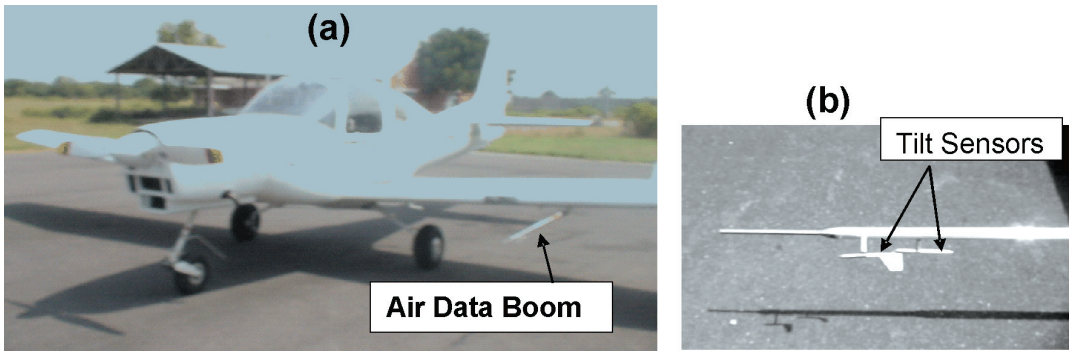

Figure 7. (a) Photograph of the HANSA-3 aircraft used to record free flight FST;
(b) The air-data boom used for the measurement of velocity along with the tilt sensors.

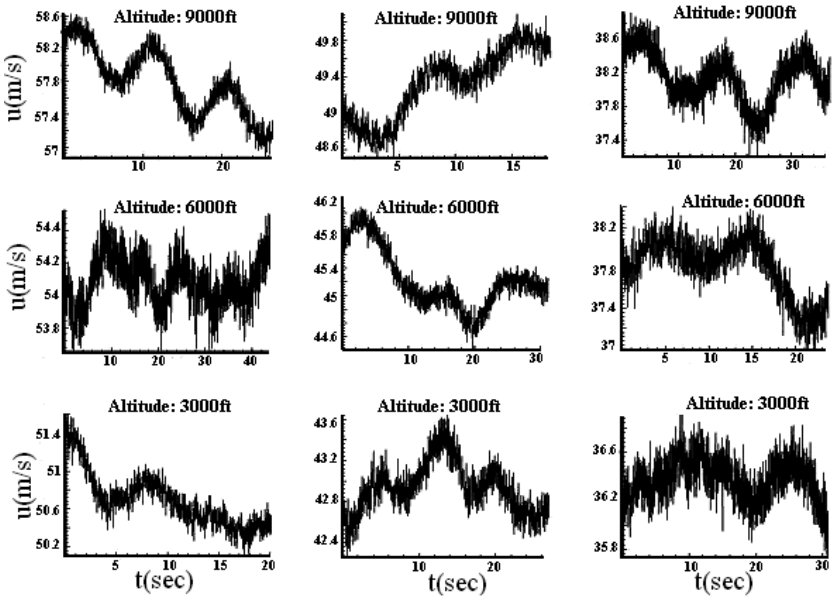

Figure 8. Time-record of measured in-flight freestream velocity for three different cruising speeds at three altitudes.

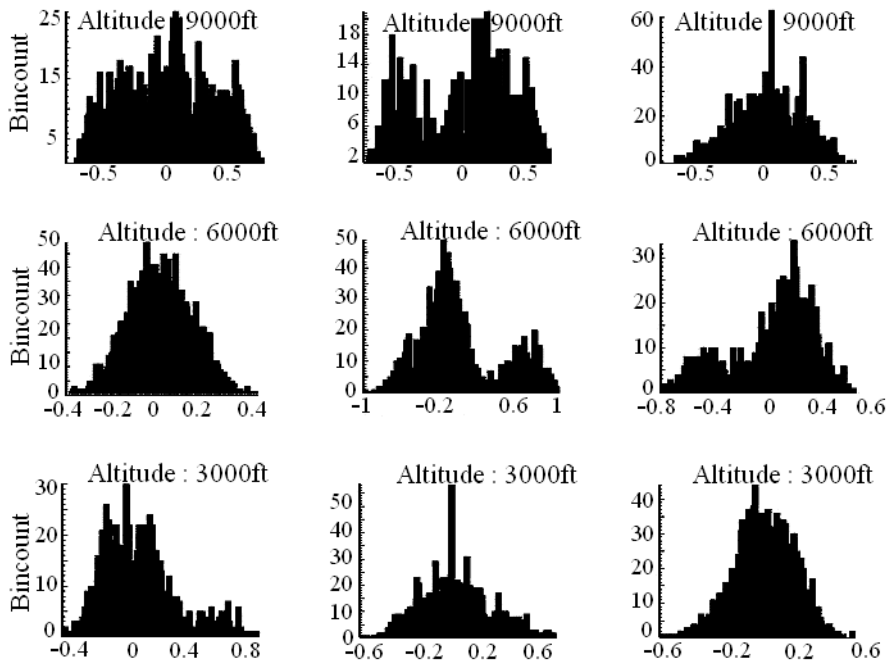

Figure 9. PDF of measured in-flight disturbance freestream velocities of Figure 8.

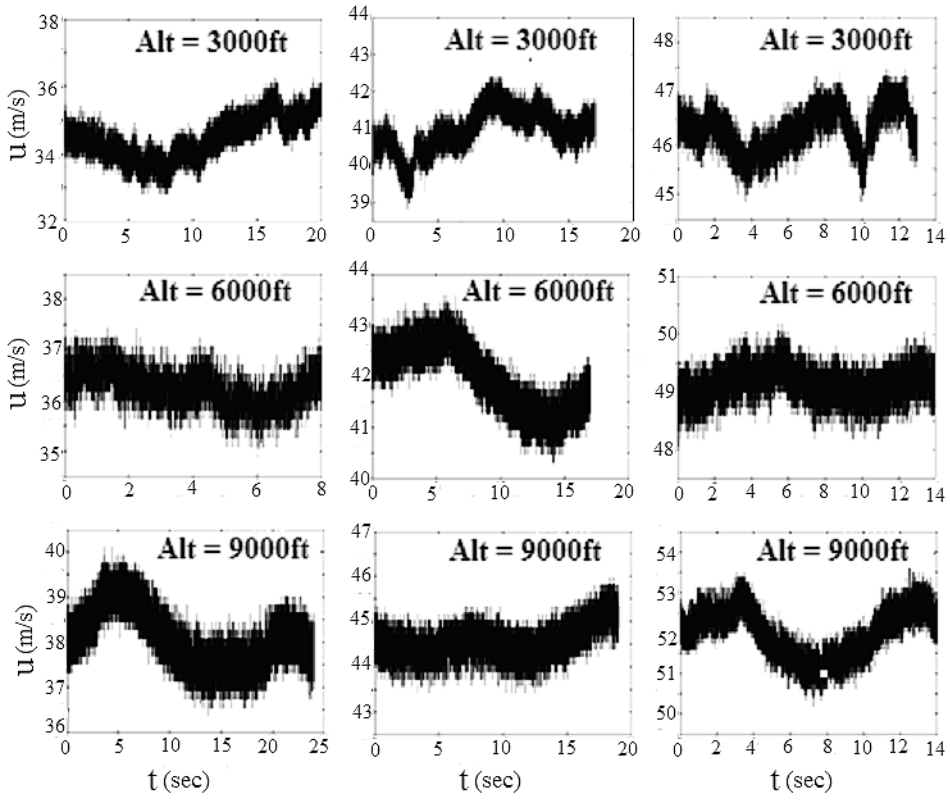

Figure10. Measured in-flight freestream velocity time-record for three different cruising speeds at three altitudes on a different day, as compared to the data collected for Figure 8.

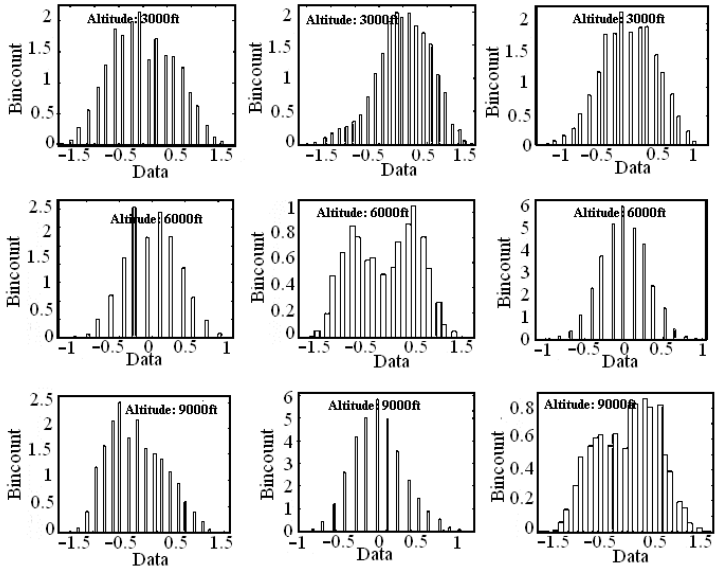

Figure 11. PDF of measured in-flight disturbance freestream velocities shown in Figure 10.

Having obtained the time-series for the background disturbance data from wind tunnel and flight tests, their statistics are compared in Figure 12 as a function of wind speed. In Figures 8 and 10, the flight data are shown for the indicated altitudes and the statistics show similar range for the respective quantities. It is noted that for the wind tunnel, *Tu* changes discontinuously across 50cm/s wind speed. For lower speeds, the tunnel has significant variations about the mean speed. While the wind tunnel displays maximum *Tu* of about 1.4% for a free stream speed 40cm/s, for the flight data this is always below 0.9% for the April data. During the dry period, *Tu* progressively comes down as one ascends to higher altitudes. However, in the presence of unsteadiness (gust) of the free stream one would have significantly higher *Tu* and skewness- as seen in the September data shown in Figure 12.

To assess the role of scalewise contribution to various moments of the wind tunnel FST, the second, third and fourth moments for the full and the high-pass data have been compared in Figure 13. It is observed that the moments for the full data appear without any pattern, while the high-pass data shows definitive trend in its variation for the even moments. For example, the high wave number contribution to turbulent intensity (*Tu*) of the empty tunnel is roughly about 10% of the total value, as shown in the plot of Figure 13- as a function of tunnel speed. The tunnel displays discontinuous *Tu* for flow speed exceeding 40cm/s. The fourth moment of the full- and high-pass data also show that the high wave number components contribute by a small fraction to the overall value with discontinuous jump across 40cm/s speed. The high-pass data show an increase in fourth moment to increase nonlinearly with speed up to 40cm/s and thereafter it falls suddenly, to increase further again from the low value for further increase in speed. Also, the randomness of the third moment indicates significant unsteadiness of the tunnel speed at high frequencies.

For the Karman vortex shedding, the dynamics is essentially determined by the sufficient forcing at the relatively lower Strouhal frequency, as seen via variations with *Tu* only. However, presence of higher order statistics – mainly the skewness indicates vortex stretching [30] and thus, implies a higher frequency-rich spectrum. These higher frequencies can trigger Kelvin-Helmholtz and other instabilities that will be discussed later with respect to a bluff body simulation. Thus, in general it is important to model the higher order statistics correctly to capture all possible instability modes and even stochastic forcing at higher wave numbers and frequencies in a flow.

The tunnel used for the present exercise operates with large-scale fluctuations at speeds lower than 40cm/s. In an experiment, this large scale unsteadiness can manifest in exciting flow instabilities significantly. Figures 12 and 13 clearly show that all moments are dominated by large scale events, with the third moment or skewness playing a major role. It has been noted [30] that skewness of velocity signal indicates forward scatter via vortex stretching and for homogeneous turbulence it should be negative, if the time rate of change of enstrophy due to nonlinear interactions is positive.

Above mentioned unsteady nature of the oncoming flow in a wind tunnel at low speeds was seen from the histogram of the empty tunnel velocity data in Figures 4 and 5. Bin counts for the two velocities in these figures, show multi-modal distribution. In Juel at al. [31], such multi-modal histogram has been identified with the effects of noise on the dynamics near bifurcation- an indication of evolving or time-varying flow (at low frequencies) inside the empty tunnel itself.

Flight data in Figures 8 and 9 also show behavior similar to that of wind tunnel data observed in Figures 4 and 5. Low frequency fluctuations are observed along with high frequency random fluctuations. The level of turbulence intensities are of the order 1% for both the flight and the wind tunnel data. PDFs of the flight data are non-Gaussian, with skewness and kurtosis values similar to that in wind tunnel data. Thus, the nature of the in-flight and wind tunnels FST appears to be similar. Hence, in modeling FST, presence of the low frequency components is required besides the high wave number and frequency components determined by higher order statistics. This is discussed in the following section.

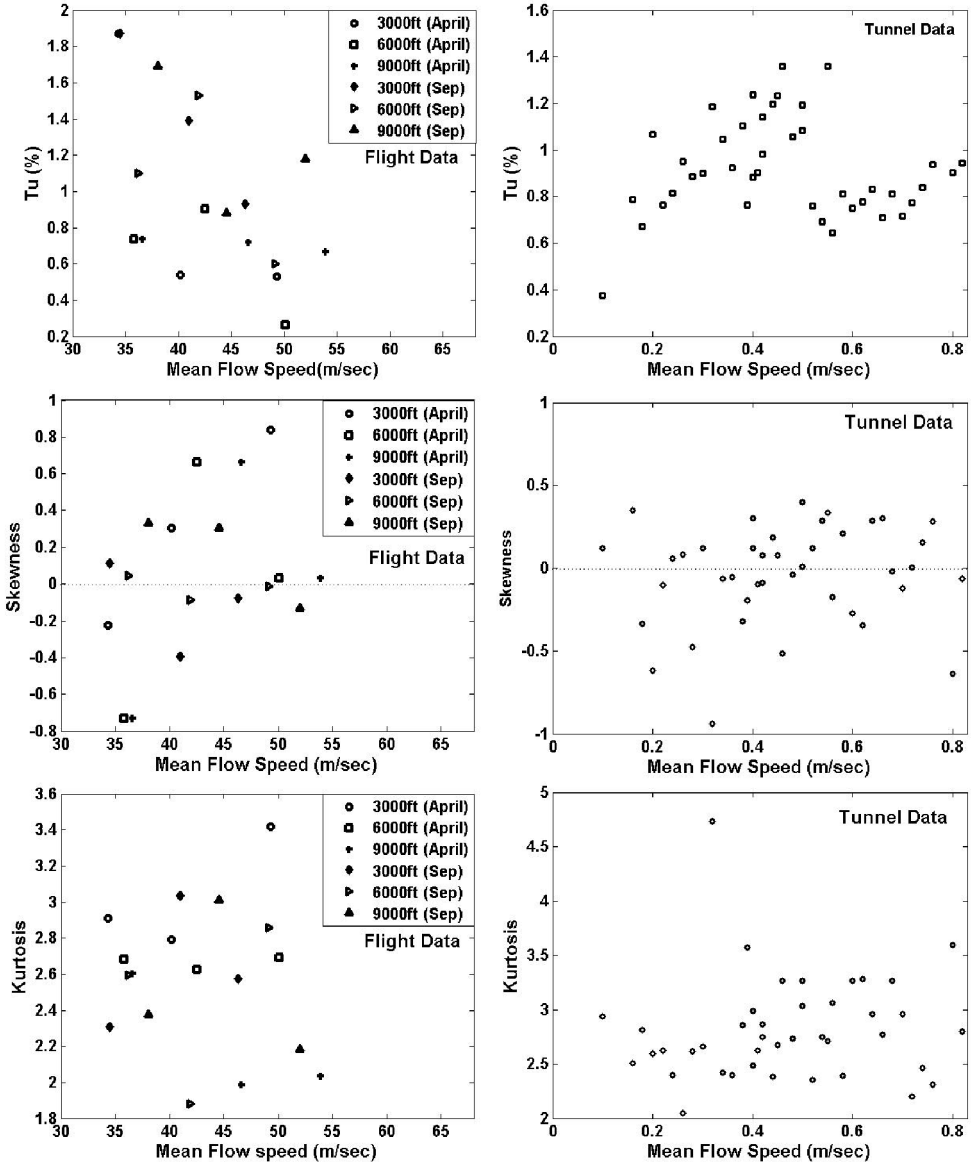

Figure12. Comparison of turbulence intensity (top), skewness (middle) and kurtosis (bottom) of flight (left) and wind tunnel (right) data.

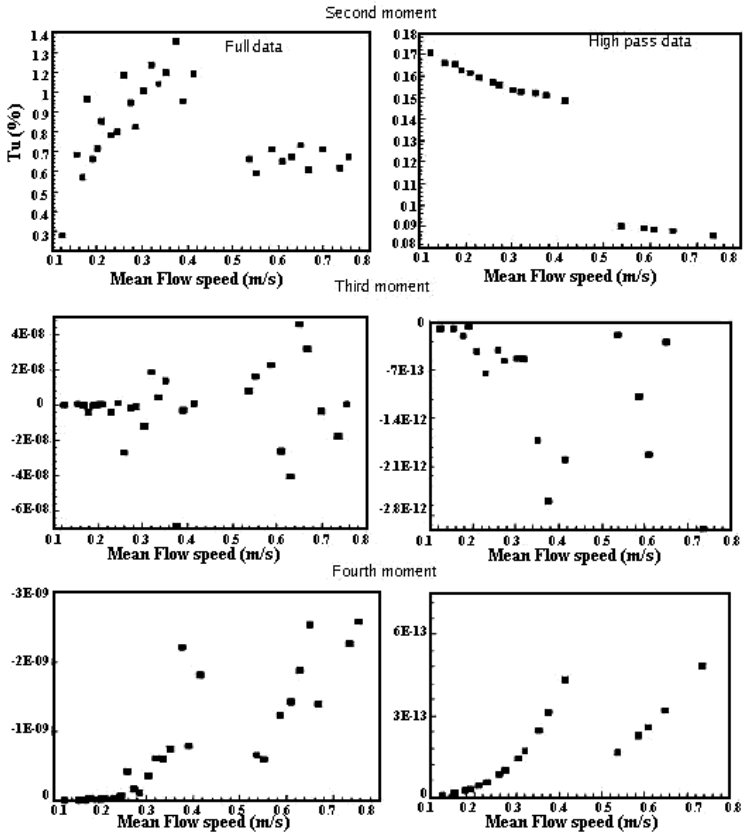

Figure 13. Contribution of high wave number components to second, third and fourth order moments of wind tunnel noise data shown on right, as compared to full data on left.

4. STOCHASTIC MODELING OF FST

Discussions in the previous sections indicate the need to model FST, taking into account the presence of large-scale, low-frequency flow structures with the oncoming flow. A preliminary attempt was made in [15], where FST was modelled using a first order moving average model [32]. That model was proposed based on the observation in [16] that reported the histogram of a specific wind tunnel with an essentially symmetric PDF. As the skewness of such a histogram is zero, in the moving average model the parameters of the FST model was fixed by matching the second and fourth moments of the tunnel data to that of the model only, while assuming the skewness to be zero. Presented results here indicate the need to include the skewness in the FST model. The simulation of Navier-Stokes equation with this improved FST model will be more realistic than solving any stochastic differential equation for a laminar flow [14].

Here, a model that takes into account the low frequency data of the FST, as obtained experimentally, is proposed. In this moving average model, the streamwise disturbance component of velocity field is represented by,

$$u' = e_t + \alpha e_{t-1} + \sum_{j=1}^{N} a_j e^{ik_j(x-ct)} \tag{4}$$

where the first two terms are given by a Gaussian distribution at successive time steps with unknown standard deviation (σ), and the last term stands for the low frequency component of the noise (as shown e.g., in Figure 3) that is facility- and speed-dependent; c is the phase speed of propagation of these low wave number coherent structures. Using such models at the inflow of a computational domain to provide the background disturbance for solving Navier-Stokes equation, the exact value of c is found not to be very important.

In the FST model, the large-scale anisotropy of the oncoming flow is retained up to a low frequency range, as in the FFT of the empty tunnel record at the same speed. These would account for the skewness of the data shown in Figure 12. The moving average time series of order one [32] is used to obtain the Gaussian distribution in equation (4), second and fourth moments of which, are fixed in such a way that the composite signal's moments match with the high-pass experimental time series. This way, one constructs an FST model corresponding to the actual flow in the experiment. In Figure 14, FFT of the experimental wind-tunnel data for the disturbance velocity is compared to the synthetically generated FST using equation (4), for the mean flow speed of 17cm/s. It is evident from this figure that the major peaks of FFT of the actual data are retained in the synthetic FST model, all the way up to frequency of 200 Hz. It is done purposely, as the proposed FST model has been used for computing flow past a circular cylinder. The essential aim is to retain the FST signature up to and above the Strouhal number of Karman vortex shedding (KVS). Note that the frequency near 50Hz is not an electrical noise frequency. The value of this frequency is 47Hz, whereas; the line frequency is exactly equal to 50Hz. In performing this exercise, we note that the KVS is related to an instability of the wake bubble with a pair of opposite signed vortices in it and the instability causes shedding of the vortices alternately at lower frequency. This is usually simulated without the need for any background excitation, i.e., the numerical errors associated with truncation and round-off is sufficient to initiate this instability. However, in a noisy flow with FST, the system dynamics can be significantly altered by the constant excitation at many frequencies simultaneously with finite amplitude. In such a case, the evolving wake bubbles can also suffer Kelvin-Helmholtz instability that is investigated next.

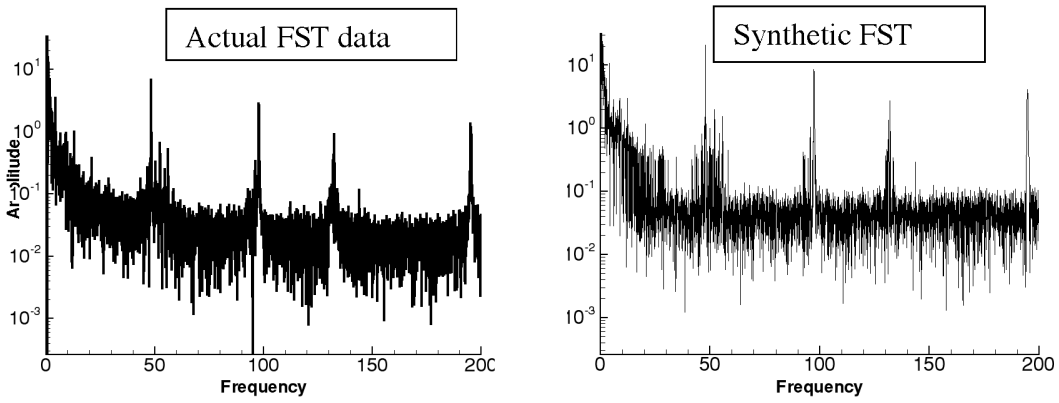

Figure 14. FFT of actual and modelled FST data obtained using equation (4).

5. COMPUTING FLOW PAST CYLINDER IN THE PRESENCE OF FST

The flow past a circular cylinder is simulated here for transcritical Reynolds numbers for which the flow has shown sensitive dependence on background disturbances. For example, experiments of Homann [23] in an oil-tunnel showed no shedding of vortices below Re = 65, due to absolute quiet nature of the flow in that special tunnel.

The formulation and the numerical methods employed in the present simulation are same that is reported in [33]. Here, the two-dimensional Navier-Stokes equation is solved in the stream function (ψ) – vorticity (ω) formulation in a polar domain with the outer boundary placed at twenty diameter distance from the centre of the cylinder. The nonlinear convection terms in the vorticity transport equation is discretized using a high accuracy compact scheme and the time marching is performed using four- stage Runge- Kutta method [33].

In Figure 15, computed flow with the FST model for Re = 55 is compared with the experimental results of Homann [23]. The experimental results [23] in Figure 15(a) show absence of shedding, and the near-wake symmetry, while some undulations are noted in the far wake. For the FST model, a very low value of $Tu = 0.001$ has been prescribed at the inlet of the computational domain with the oncoming flow, with the understanding that the flow in [23] had very little background noise. With the FST model switched-on, the computed results match with the experiments in most details – the undulation of the far-wake is related to low frequency pulsation of the near-wake bubbles caused by the imposed noise.

The events seen in Figure 15, shows an undulating wake without the alternately shed vortices from the cylinder wall as is usually the case for KVS. Instead, the primary wake-bubble is seen continuously here in the near-wake and the limiting streamline constituting the edge of the recirculating bubble is a thin vortex sheet excited by FST via the Kelvin-Helmholtz instability (KHI) mechanism. This causes the sheet to undulate and a small quantity of vorticity is released in the wake periodically. This periodic stripping of small quantity of vorticity will show up as unsteadiness in the measured signal in the wake. It is expected that the KHI events would occur at small scale and that corresponds to higher frequencies in the spectrum.

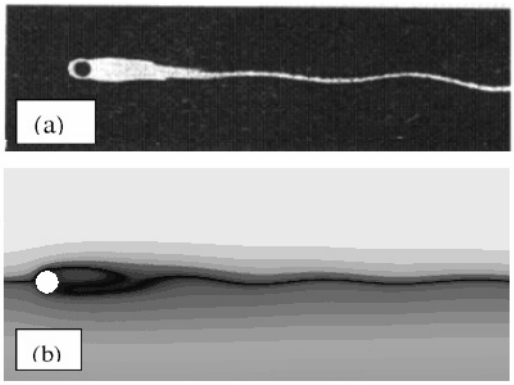

Figure 15. (a) Experimental results due to Homann [23] for Re = 55 obtained in an oil-tunnel, (b) Present computed result with the FST model as given by equation (4) with turbulent intensity, Tu = 0.1%.

To understand the role of disturbances in causing KVS and KHI, another case is computed for Re = 53, exposed to higher levels of FST. These results are shown in Figure 16, where the computed vorticity contours are shown plotted for Tu = 0.5% (top) and 1.5% (bottom), respectively. For the displayed cases, the maximum and the minimum values of vorticity are noted in the frames. It is interesting to note that for the lower FST case, the magnitude of maximum and the minimum values occurring near the wall are almost the same. This implies the near symmetry of the vorticity field, although there is asymmetry in the far-wake with the formation length significantly high. Also, it is noted that the vorticity values are twice for the lower Tu case, as compared to the higher Tu case. This is also due to the symmetry of the bubble and the larger formation length that allow vorticity evolution to higher values without shedding. In contrast, for the higher FST case, the turnover time for each cycle is shorter because of the larger amplitude of excitation field that causes quicker stripping of vorticity and the loss of symmetry earlier. For both the cases, the synthetic FST is created while matching the Tu values. For the lower FST case, the solution is shown for t = 230, at a time where one can notice alternately shed vortices. This is similar to the case shown in Figure 15, where none of the wake-bubbles are detached completely at any time and only weak vortices are shed from the tip of the attached primary wake-bubble. However, the strength of FST is five times higher and the stripped vortices are of larger dimension, even though their strength is significantly lower. The displayed solution for the higher FST case is shown at t = 203.

The above description of the flow field can also be seen in the time history of the lift experienced by the cylinder in each case, as shown in Figure 17. The lift and drag (not shown here) values are derived from the calculated vorticity field by solving the vorticity transport equation and the pressure field obtained by solving the Poisson equation for the total pressure – a description of the equation and solution method is also given in [33]. The latter is required for the correct evaluation of the total pressure field – that being a good measure of mechanical energy of the flow. The total pressure reduces to the static pressure on the no-slip surface of the cylinder that allows calculating its contribution to lift and drag.

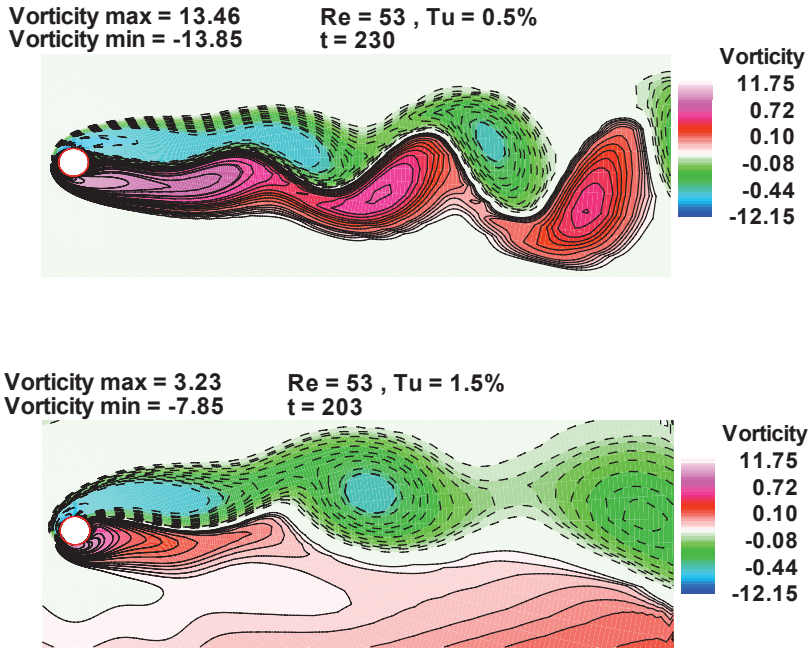

Figure 16. Computational vorticity contours for Re = 53 case with Tu = 0.5% (top) and Tu = 1.5% (bottom). Maximum and minimum values of vorticity are also marked for both the cases. The solid lines indicate positive vorticity and the dotted lines indicate negative vorticity.

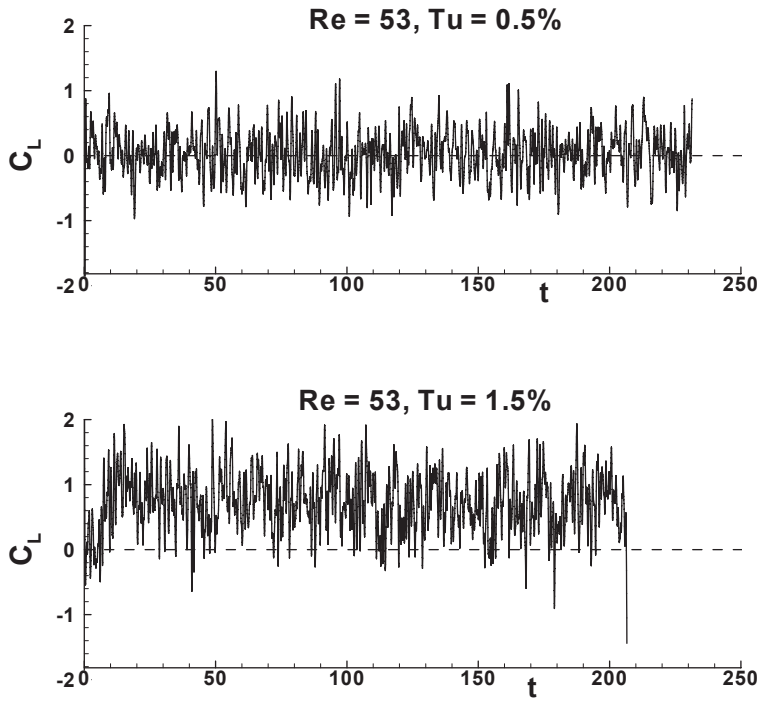

Figure 17. Time-variation of lift coefficient for the computed cases shown in Figure 16.

Displayed lift variation does not immediately show any preferred time scales or frequencies – due to the absence of any apparent periodicity in the time series. Also, it is noted that the time average of lift is quite different for these two cases. This is due to the different vorticity dynamics in each case- as discussed above with respect to Figure 16 results. The computed results in a domain of radius that is 20 times the cylinder diameter show a strong coupling between the vortical field of the incoming flow with the vorticity generated at the no-slip wall, when the FST level of the oncoming flow is large (Tu = 1.5 %). For the lower FST case (Tu = 0.5 %), the interaction is much weaker and the flow field retains its top-down symmetry- as noted by the zero mean lift in Figure 17. Higher FST levels bring about an effect that is similar to an incoming flow with mean shear present.

The dominant time scales for these cases are seen in Figure 18 that is the Fourier transform of the lift time series shown in Figure 17. In this figure, the Fourier amplitude is plotted in the log-scale against a non-dimensional frequency. For the case of Re = 53, the Strouhal frequency is marked by a vertical arrow-head that occurs at St = 0.12. For the lower FST case, we note two peaks, marked as A and B, with the latter having a larger amplitude. The lower peak at A is closer, but slightly lower as compared to the Strouhal frequency. This slight de-tuning is due to the presence of noise – a typical feature of non-linear systems, see e.g., Juel et al. [31] and other references contained therein that discuss the effects of noise on system dynamics. Also for the higher FST level case, the most significant peak at A occurs at a frequency lower than the Strouhal frequency. This frequency for the higher FST case is slightly lower than that for the lower FST case – showing that the detuning increases with the increase in the amplitude of noise.

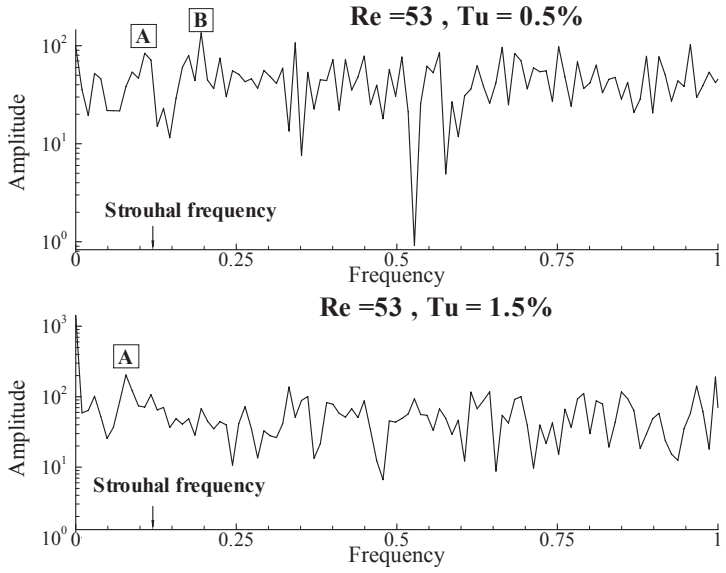

Figure 18. Fourier transform of the lift data shown in Figure 17. The Strouhal frequency is marked for reference by a vertical arrow-head, in both the figures.

The presence of the second peak, for the lower FST case at B has higher amplitude, as compared to the amplitude at A. These events at higher frequencies are caused by the stripping of vortices from the wake-bubble by the FST that tries to destabilize the equilibrium symmetric wake-bubble configuration. But that is not strong enough to completely dislodge any one of the wake vortices completely. This is readily evident from the maximum positive and negative vorticity values computed for the two FST cases in Figure 16. For Tu =1.5% case, wall vorticity does not attain even the 50% value as compared to the case of Tu = 0.5% and is symptomatic of vortex stripping by FST. This stripping process occurs at a faster pace, as compared to the overall shedding of larger vortices alternately in the wake. When the FST level is increased to Tu = 1.5%, the symmetric wake-vortices configuration is destabilized, thereby causing vortices to be shed at a faster rate from the near vicinity of the cylinder and hence the second peak is not seen. Thus, the higher FST seems to accelerate the KVS phenomenon that prevents the occurrence of KHI – which is seen for lower FST cases.

6. CONCLUSIONS

Present interest in studying the effects of free stream turbulence (FST) on flow instability and transition is represented here by a set of multiple activities. Past studies reveal that instabilities of flows sensitively depend upon background disturbances, but the models based on experimental FST characteristics have not been developed. The need for this approach is established via the results of Figure 1, where the same Reynolds number flow is established in the same wind-tunnel by choosing two different diameter cylinders kept at two different free stream speeds. The different shedding patterns seen for the same Reynolds number for the flow past a geometrically smooth cylinder, establishes the central role of background disturbances.

Compared to solving the problem as a stochastic laminar flow [14], in the present approach the extrinsic dynamics of the flow is calculated with respect to the model of actual FST measured from wind-tunnel and flight experiments at different altitudes. In the first part of the work, background noise data collected from these two sources are characterized in terms of their statistics, up to the fourth order. Presented data in Figures 4 to 12, show similarity between wind-tunnel FST and measured disturbances in flight experiments at relatively lower altitudes. The second and the fourth order statistics of the actual high-pass data has been matched in constructing a synthetic time series using the moving average method of order one [32] and to this FFT of the actual wind-tunnel data at lower wave numbers has been added to simulate the skewness of the background noise. This results in a good match of the synthetic FST model with the actual FST data- as shown in Figure 14.

In the final part of the work, the developed model of FST is used for calculating flow past a circular cylinder and the results are compared with the experimental results of Homann [23] in Figure 15. The visualized flow of [23] at Re = 55 is computed as a flow experiencing very low FST of Tu = 0.1%. Extrinsic non-linear dynamics of the flow is studied further for Re =53 by considering two higher FST levels of Tu = 0.5% and 1.5%. Various results are shown in Figures 16 to 18 to bring out the characteristics of such flows. The role of Kelvin-Helmholtz instability at lower FST level that shows the presence of two peaks for the lower FST case is established. One corresponds to alternate vortex shedding at a lower frequency (with respect to Strouhal number), and the other occurring at higher frequency due to Kelvin-Helmholtz instability. For larger FST level, these latter events are not dominant and one sees a predominant peak near the Strouhal number. Detuning of the predominant frequency from the Strouhal number due to non-linearity has also been noticed. This establishes the need to study these problems with respect to actual FST present in the experiments.

ACKNOWLEDGEMENTS

Authors acknowledge the help of pilot and staffs of Flight Laboratory, Dept. of Aerospace Engineering, IIT Kanpur - particularly Mr. Ankur Singhal- for conducting all the in-flight experiments and providing us with the data.

REFERENCES

[1] Dutton, J. A. & Hans, A. P. Clear Air Turbulence: A mystery may be unfolding: High altitude turbulence poses serious problems for aviation and atmospheric science, *Science,* 1970, 167, 937-944

[2] Taylor, G. I. & Batchelor, G. K. The effect of wire gauze on small disturbances in a uniform stream, *Quart. J. Mech Appl Math.* 1947, 2, 1-29

[3] Baines, W. D. & Peterson, E. G. An investigation of flow through screens, *Trans. ASME,* July 1951, 73, (5), 467-480.

[4] Lumley, J. L. & Mc Mahon J. F., () Reducing water tunnel turbulence by means of a honeycomb, *Trans. ASME, Ser. D., J. Basic. Eng.* 1967, 89, 764-770.

[5] Loehrke, R. I . & Nagib H . M., Control of free-stream turbulence by means of honeycombs: a balance between suppression and generation, *Trans. ASME, J. Fluids. Engg.,* 1976, 98, 342-353.

[6] Mikhailova, N. P., Repik, E. U. & Sosedko, Yu. P. Optimal control of free-stream turbulence intensity by means of honeycombs, *Fluid Dynamics,* 1994, 29(3), 429-437

[7] Derbunovich, G. I., Zemskaya, A. S., Repik, E. U. & Sosedko, Yu. P., Use of screens for controlling the structure of flow turbulence in wind tunnels, *Uch Zap TsAGI,* 1982, 13, 11-14.

[8] Schmid, R., Stuff, R., Klein, U. K. A., Jamjoon, F. A. & Al-Suwaiyan A., Low free-stream turbulence in test sections through packed beds and fibrous mats, *Expts. in Fluids,* 1999, 26, 451- 459.

[9] Wojno, J.P., Mueller, T. J., and Blake, W.K., Turbulence ingestion noise Part II: Rotor aeroacoustic response to grid-generated turbulence, *AIAA Journal*, 2002, 40(1), 26-32.

[10] Mueller, T.J., Pohlen, L.J., Cnigliaro, P.E. & Jansen Jr., B.J., The influence of free-stream disturbances on low Reynolds number airfoil experiments, *Expts. in Fluids*., 1983, 1, 3-14.

[11] Pope, S.B., *Turbulent Flows*, Cambridge Univ. Press, Cambridge, U.K. 2000.

[12] Kwok, C. S. Kenny, Turbulence effects on flow past circular cylinder, in *Recent Advances in Engineering Mechanics and Their Impact on Civil Engineering Practice*, (Eds: W. F. Chen and A. D. M. Lewis), *New York:* 1981, 1224-1227

[13] Pal, S. & Raj. J., Wake behavior in the presence of free stream turbulence, *Trans. Of ASME, J of Engineering for Power*, 1991, 103, 490-498.

[14] Lucor, D. & Karniadakis, G.E., Noisy inflows cause a shedding-mode switching in flow past an oscillating cylinder, *Phys. Rev. Letters,* 2004, 92, 154501-1 154501-4.

[15] Sengupta, T.K., De, S. & Gupta, K. Effect of free-stream turbulence on flow over aerofoil section at high incidence, *J. Fluids & Struct*., 2001, 15, 671-690.

[16] Frisch, U., *Turbulence*, Cambridge University Press, Cambridge, U.K. 1995.

[17] Spark, E.H. & Dutton, J.A., Phase angle considerations in the modeling of intermittent turbulence, *J. Atmosph. Sc.* 1972, 29, 300-303.

[18] Edwards, S.F., The statistical dynamics of homogeneous turbulence, *J. Fluid Mech*., 1964, 18, 239-273.

[19] Syono, S. & Tanaka, H., () On frequency distribution of wind speed and direction in turbulent flow, *J. Meteor. Soc. Japan*, 1966, 44, 89-100.

[20] Batchelor, G. K., *An Introduction to Fluid Dynamics*,1st Indian Ed. Cambridge Univ. Press, New Delhi, 1993.

[21] Landau, L. D. & Lifshitz, E. M., *Fluid Mechanics*, 2nd Ed. Butterworth & Heinemann, Oxford, 1989

[22] Kovasznay, L.S.G., Hot-wire investigation of the wake behind cylinders at low Reynolds numbers, *Proc. Roy. Soc. London A*, 1949, 198, 174-190.

[23] Homann, F., Einfluss groesser zaehigkeit bei stroemung um zylinder, *Forschung auf dem Gebiete des Ingenieurwesens,* 1936, **7**(1), 1-10.

[24] Roshko, A., On the drag and shedding frequency of two-dimensional bluff bodies, *NACA TN,* 1954, 3169.

[25] Kiya, M., Suzuki, Y., Mikio, A. & Hagino, M., A contribution to the free stream turbulence effect on the flow past a circular cylinder, *J. Fluid Mech*., 1982, 115, 151-164.

[26] Zebib, A, Stability of viscous flow past a circular cylinder, *J. Eng. Math.,* 1987, 21, 155-165.

[27] Morzynski, M. & Thiele, F., Numerical investigation of wake instabilities, In *Bluff-body Wakes, Dynamics and Instabiilties (eds. Eckelmann, Graham, Huerre & Monkewitz),* Springer Verlag, Berlin, 1993.

[28] Schlichting, H., *Boundary Layer Theory*, 7th Ed. McGraw-hill, New York, 1979.

[29] Freedman, D. and Diaconis, P. On the histogram as a density estimator: L2 theory. *Probability Theory and Related Fields*, 1981, 57(4), 453-476

[30] Batchelor, G.K. & Townsend, A. A., Decay of vorticity in isotropic turbulence, *Proc. Roy. Soc. (London) A*, 1947, 191, 534-550.

[31] Juel, A., Darbyshire, A.G. & Mullin, T., The effect of noise on pitchfork and Hopf bifurcations, *Proc. Roy. Soc. (London) A*, 1997, 453, 2627-2647.

[32] Fuller, W.A., *Introduction to Statistical Time Series*, Wiley, New York, 1978.

[33] Dipankar, A., Sengupta, T.K. & Talla, S.B., Suppression of vortex shedding behind a circular cylinder by another control cylinder at low Reynolds numbers, *J. Fluid Mech*., 2007, 573, 171-190.